# Inviscid Analysis of Transonic, Slatted Airfoils

D.A. Caughey*
*McDonnell Douglas Corp., St. Louis, Mo.*

**A numerical method is presented for the analysis of the inviscid flowfields about airfoils with leading-edge slats operating in the transonic speed regime. The method is based upon a previously developed, small-disturbance theory for transonic airfoils, utilizing the geometrical advantages inherent in a preliminary conformal mapping to the complex potential plane of the incompressible flow about the body. In the current study, the mapping is performed for the main airfoil alone; the slat is incorporated using thin airfoil theory to displace the point of application of the slat boundary conditions to the nearest coordinate line of the computational grid. The finite-difference analog of the resulting equation for the perturbation potential is solved using type-dependent line overrelaxation. Arbitrary slat-airfoil combinations can be treated, and agreement with experimental data is quite good for cases in which viscous effects on the slat are not too important.**

## Nomenclature

$a$ = speed of sound

$a(\phi,\psi)$, $b(\phi,\psi)$, $c(\phi,\psi)$, $d(\phi,\psi)$ = coefficients in quasi-linearized equation

$c$ = airfoil chord
$C_{l_w}$ = main airfoil lift coefficient
$C_p$ = pressure coefficient
$f$ = scaling function in $\psi$-direction
$g$ = scaling function in $\phi$-direction
$M_\infty$ = freestream Mach number, $= U/a_\infty$
$P$ = perturbation velocity potential
$PF$ = nonlinear coefficient in potential equation
$Q$ = magnitude of incompressible velocity vector
$s$ = independent variable in $\psi$-direction in computational plane
$t$ = independent variable in $\phi$-direction in computational plane
$U$ = freestream velocity
$x$ = coordinate in freestream direction
$x_n$ = distance from nose of main airfoil
$\beta$ = Prandtl-Glauert parameter, $= (1-M_\infty^2)^{1/2}$
$\gamma$ = specific heat ratio
$\Gamma$ = incompressible circulation about airfoil
$\Gamma_s$ = slat circulation
$\Gamma_t$ = total contribution to circulation due to compressibility and slat
$\delta$ = small parameter in transonic limit
$\theta$ = slat surface angle, relative to local incompressible streamline
$\phi$ = incompressible velocity potential, $= Re(\Phi_i)$
$\Phi$ = velocity potential
$\Phi_i$ = complex incompressible velocity potential
$\psi$ = incompressible stream function, $= Im(\Phi_i)$
$\psi_{sl}$ = value of $\psi$ most closely approximating location of slat

*Subscripts and Superscripts*

$\overline{(\ )}$ = normalized quantity in transonic limit
$(\ )_\infty$ = freestream value
$(\ )^+$ = value on upper surface of slat
$(\ )^-$ = value on lower surface of slat

Presented as Paper 74-541 at the AIAA 7th Fluid and Plasma Dynamics Conference, Palo Alto, California, June 17-19, 1974; submitted June 21, 1974; revision received March 14, 1974. This paper summarizes work performed under the McDonnell Douglas Independent Research and Development Program.

Index categories: Subsonic and Transonic Flow; Aircraft Aerodynamics (including Component Aerodynamics).

*Scientist, Flight Sciences Department, McDonnell Douglas Research Laboratories; currently Assistant Professor, Sibley School of Mechanical and Aerospace Engineering, Cornell University. Member AIAA.

## Introduction

In the design of high-performance aircraft, the simultaneous constraints of efficient high-speed cruise and good transonic maneuverability necessarily result in performance-limiting compromises. The extent of these limitations can be considerably reduced by permitting the aerodynamicist greater flexibility in the geometric configurations he is allowed to employ. One such avenue of greater flexibility is the use of fixed or variable-geometry, multi-element lifting surfaces. In particular, one promising area of interest to designers of high-performance aircraft is that of the transonic, or maneuvering, slat. Such devices, if properly designed, hold the promise of greatly increased buffet-free transonic lift coefficients while not significantly detracting from high-speed cruise efficiency.

Several methods exist[1-4] or are currently under development[5] for treating either exactly or approximately the inviscid flow about multi-element airfoils in the incompressible flow regime. Unfortunately, all of these methods rely upon either conformal mapping techniques or surface singularity methods, and are therefore not directly applicable to compressible flows. The present method attempts to fill this requirement, i.e., to provide the aerodynamicist with a tool for analyzing the inviscid, transonic flow about slat-airfoil combinations.

## Analysis

### Small-Disturbance Theory

The basis for the present study is a small-disturbance form of the potential equation, derived in the complex potential plane of the incompressible flow about the main airfoil to be analyzed.[6] This choice of independent variables is motivated by the requirements that 1) the airfoil surface reduce to a coordinate line for exact application of the boundary conditions there, and 2) the coordinate system be amenable to a simple description of the limiting flow in the perturbation analysis. The first requirement is satisfied, as the body

reduces to a portion of the real axis in the complex potential plane, while the second will be satisfied by choosing the incompressible velocity field as the limiting flow for the perturbation analysis.

The complete nonlinear equations of perfect fluid flow for the case in which a velocity potential exists may be reduced to the form

$$a^2 \nabla^2 \Phi = \nabla \Phi \cdot \nabla (\tfrac{1}{2} \nabla \Phi^2) \tag{1}$$

where $\Phi$ is the velocity potential and $a$ is the speed of sound, which must be related to the velocity potential by means of the Bernoulli equation. For the homoenergetic flow of a calorically perfect gas of specific heat ratio $\gamma$, this may be written

$$a^2 = a_\infty^2 + \frac{\gamma - 1}{2} \{ U^2 - \nabla \Phi^2 \} \tag{2}$$

where $U$ is the freestream velocity and the subscript $\infty$ refers to conditions in the freestream. The existence of a velocity potential is guaranteed, at least to terms of second order, in the classical transonic small-disturbance theory[7] and is a great convenience for use in relaxation schemes.

The perturbation potential $P$ is introduced as a measure of the departure of the solution from the incompressible potential as follows:

$$\Phi = U\{ \phi + M_\infty^2 P(\phi, \psi) \} \tag{3}$$

where $M_\infty = U/a_\infty$ is the freestream Mach number and $\phi$ and $\psi$ are, respectively, the real and imaginary parts of the incompressible potential function, $\Phi_i = \phi + i\psi$. The perturbation theory for Eqs. (1) and (2) is now developed under the simultaneous constraints that 1) an orderly expansion of the Janzen-Rayleigh type is obtained in the limit as the Mach number vanishes, and 2) a nontrivial transonic limit is obtained under a multiple-limit process whereby the incompressible velocity field approaches a uniform value while the Mach number approaches unity.

Substitution of Eq. (3) into Eqs. (1) and (2) then yields the "universal" equation

$$\{ 1 + \frac{\gamma - 1}{2} M_\infty^2 (1 - Q^2) \} P_{\psi\psi} + \{ 1 - M_\infty^2 Q^2 + \frac{\gamma - 1}{2} M_\infty^2 (1 - Q^2) - (\gamma + 1) M_\infty^4 Q^2 P_\phi \} P_{\phi\phi} = \tfrac{1}{2} \frac{\partial Q^2}{\partial \phi} + \frac{3}{2} M_\infty^2 \frac{\partial Q^2}{\partial \phi} P_\phi + \tfrac{1}{2} M_\infty^2 \frac{\partial Q^2}{\partial \psi} P_\psi \tag{4}$$

where $Q$ is the magnitude of the incompressible velocity, which is assumed known for our purposes as a function of $\phi$ and $\psi$. In the limit as $M_\infty \to 0$, Eq. (4) contains the classical Janzen-Rayleigh limiting form, up to and including terms of second order. On the other hand, in the multiple limit defined by

$$\delta \bar{P} = P \tag{5a}$$

$$\delta \bar{M}_\infty = 1 - M_\infty^2 \tag{5b}$$

$$\delta^2 \bar{Q} = 1 - Q^2 \tag{5c}$$

$$\delta^{-\frac{1}{2}} \bar{\psi} = \psi \tag{5d}$$

the transonic limiting form

$$\bar{P}_{\bar{\psi}\bar{\psi}} + \{ \bar{M}_\infty - (\gamma + 1) M_\infty^4 \bar{P}_{\bar{\phi}} \} \bar{P}_{\phi\phi} = -\tfrac{1}{2} \frac{\partial \bar{Q}}{\partial \phi} \tag{6}$$

is found as $M_\infty \to 1$ (i.e., $\delta \to 0$). In this transonic limit, the condition on $Q$ is analogous to the requirement of vanishing thickness ratio in the classical theory. Unlike the classical theory, however, the parameter $\delta$ has no clear-cut global significance, and since no useful similitude arises from the actual limiting process, Eq. (4), in terms of the original unreduced variables, is used in the calculations. The similarity of Eq. (4) [or, equivalently, Eq. (6)] to the classical transonic small-disturbance equation is evident. The equation is quasilinear, with the sign of the coefficient of the $P_{\phi\phi}$-term determining its type. Two differences from the classical theory should be noted, however: 1) the present equation is to be solved subject to homogeneous Neumann-type boundary conditions on the body, with nonhomogeneity entering directly through the right-hand-side of the equation; and 2) the present theory is valid only when the freestream Mach number is subsonic because of the manner in which this nonhomogeneity is distributed throughout the plane.

This equation must be solved subject to the requirements that there be zero normal velocity at the airfoil surface and that the perturbations from the freestream vanish at large distances from the body. Due to the orthogonality of our coordinate system, this first condition may be formalized as

$$P_\psi = 0 \tag{7}$$

on the body surface, which is a portion of the real axis in the $(\phi, \psi)$ plane. The second condition is applied, not at infinity, but at the boundaries of a finite computational domain. These boundaries are located at a large enough distance from the airfoil that the disturbances are nearly zero, and may be represented by the lowest-order solution to the far-field approximation to Eq. (4).

$$P = -(\Gamma_f / 2\pi) \arctan (\beta\psi / \phi) \tag{8}$$

where $\beta = (1 - M_\infty^2)^{\frac{1}{2}}$ and $\Gamma_f$ is the contribution to the circulation of the compressible solution (over and above that of the incompressible solution, which is contained in the basic mapping). In addition, $P$ must be allowed a discontinuity equal to $\Gamma_f$ in crossing the body streamline downstream of the trailing edge. The magnitude of $\Gamma_f$ is determined by the Kutta condition which requires that the upper and lower surface pressures be equal at the trailing edge of the airfoil.

### Slat Boundary Conditions

Incorporation of the capability to treat slatted airfoils is simplified by the choice of the streamlines of the incompressible flow about the main airfoil (lines of constant $\psi$) as one of the independent variables of the problem. Since the streamlines of the compressible solution will not differ greatly from the incompressible ones, the assumption that a well-designed slat will cause locally small perturbations to the flow about the main airfoil alone admits the possibility of linearizing the slat boundary conditions and applying them along a single coordinate line. The use of such a mean-surface approximation for the slat boundary conditions is analogous to the treatment of boundary conditions in classical thin-airfoil theory. That such a coordinate line closely approximates the chords of slats commonly used for transonic maneuvering has been shown to be the case in most geometries treated thus far by the method. A sketch depicting one such geometry and illustrating the application of the slat boundary conditions is shown in Fig. 1.

The boundary conditions to be applied along the line $\psi = \psi_{sl}$ are that the streamline slopes immediately above and below that line equal those of the upper and lower surfaces of the slat. To lowest order, this reduces to the condition that

$$P_\psi^+ = \frac{1}{M_\infty^2} \tan \theta^+ \tag{9a}$$

$$P_\psi^- = \frac{1}{M_\infty^2} \tan \theta^- \tag{9b}$$

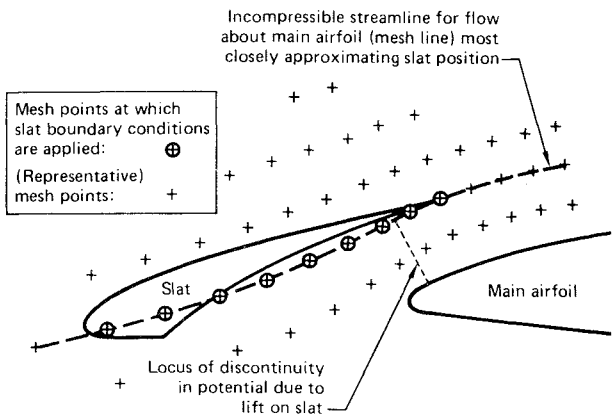


**Fig. 1 Application of slat boundary conditions in physical plane.**

where $P_{\psi}^{+}$ (or $P_{\psi}^{-}$) is the normal derivative of the perturbation potential above (or below) the line $\psi_{sl}$, and $\theta^{+}$ (or $\theta^{-}$) is the angle of the upper (or lower) slat surface relative to the grid line. Along the chordline of the slat, the line $\psi=\psi_{sl}$ is treated as a slit; values of $P$ corresponding to the upper and lower surfaces of the slat are not necessarily equal, nor does the circulation integral around the slat necessarily vanish. This latter fact allows lift on the slat and requires a discontinuity in $P$ along a line joining the slat to the point at infinity. In practice, since such a discontinuity already exists for the main airfoil along the dividing streamline leaving its trailing edge, the slat-circulation discontinuity is chosen along a line of constant $\phi$ connecting the slat and the main airfoil, with account taken of the discontinuity in the differencing formulas at neighboring points. The discontinuity downstream of the trailing edge of the main airfoil thus represents the total circulation on both the slat and the main airfoil.

## Finite-Difference Formulation

The preceding section described the analysis and formulation of the problem as a quasi-linear, partial-differential equation with its associated boundary conditions on the airfoil, slat, and in the farfield. In practice, the complexity of the equation precludes its analytical solution, even for simple geometries, and the problem must be solved numerically. This is achieved by replacing the differential equation (Eq. 4) by its finite-difference analog at a finite number of points in the plane, and solving the resultant set of (nonlinear) algebraic equations by iteration for the values of $P(\phi, \psi)$ at the given points.

For the present purpose, the mapping of the main airfoil to the complex potential plane is assumed to be known. In the numerical implementation of the theory, this mapping is carried out in two steps. First, the region exterior to the airfoil surface in the physical plane is mapped to the exterior of a circle using a slight modification of a method developed by James[8] which determines the smooth modulating function describing the nonsingular part of the velocity distribution on the circle by Fourier analysis. This is then mapped to the potential plane using the analytic relations for lifting, potential flow about a circular cylinder. This mapping of the main airfoil to the potential plane is illustrated in Fig. 2. The potential plane has a slit along the real axis on the interval $[\phi_{\min}, \infty)$, where $\phi_{\min}$ is the value of the minimum potential which intersects the body.

In addition, a slit representing the slat must be incorporated as shown in Fig. 3. At mesh points along this slit, the potential has two values, corresponding to the upper and lower surfaces of the slat. This slit is joined to that representing the main airfoil along a line of constant $\phi$. Across this line, $P$ has a discontinuity equal to $\Gamma_s$, the circulation on the slat. The value of $\Gamma_s$ is determined by the requirement that the Kutta condition be satisfied at the trailing edge of the slat.

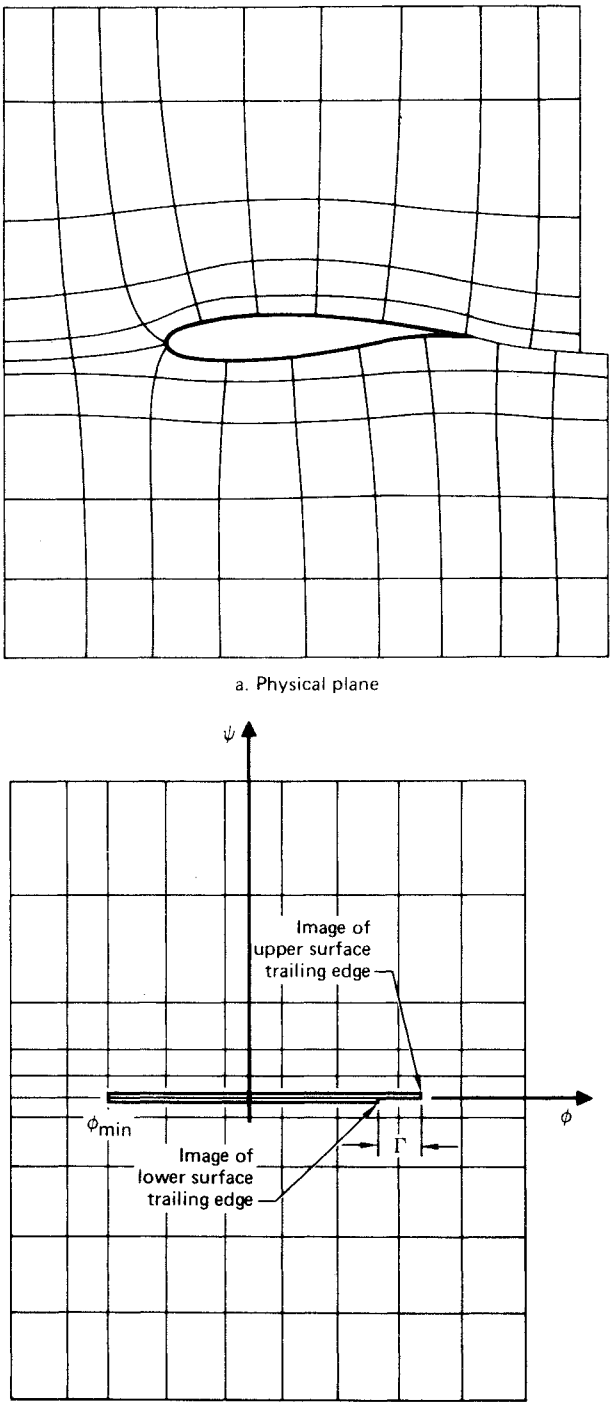


**Fig. 2 Mapping to potential plane of incompressible flow.**

### Finite-Difference Analog

For the purposes of this section, Eq. (4) may be represented in the form

$$a(\phi,\psi)P_{\psi\psi}+\{b(\phi,\psi)+c(\phi,\psi)P_{\phi}\}P_{\phi\phi} =d(\phi,\psi,P_{\phi},P_{\psi}) \tag{10}$$

where the functions $a$, $b$, $c$, $d$ may be determined by comparison with Eq. (4). For nearly all cases of practical interest, $a(\phi,\psi)$ will be everywhere positive. Thus, the equation is locally elliptic or hyperbolic depending on whether the quantity

$$PF=b(\phi,\psi)+c(\phi,\psi)P_{\phi}$$

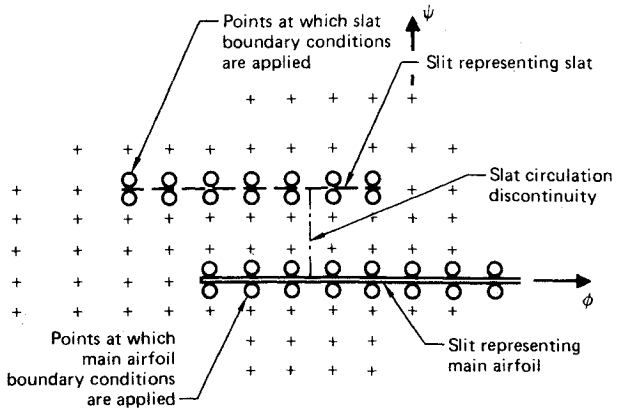


**Fig. 3 Application of slat boundary conditions in potential plane.**

is locally positive or negative, respectively. Equations of this type have been shown to be amenable to solution using relaxation techniques on their finite-difference analogs, provided the form of the finite-difference operators is allowed to reflect properly the local type of the equation.[9]

The finite-difference analog of Eq. (10) is derived by approximating the derivatives therein by finite differences of the dependent variable $P(\phi,\psi)$, at mesh points determined by the intersections of the orthogonal net $(\phi_i, \psi_j)$. To achieve the required resolution in regions of high gradients with a minimum number of mesh points, the net is not uniformly spaced, but rather, clustered near the body surface. This clustering is achieved by defining new independent variables according to the relations

$$t=g(\phi) \tag{11a}$$

$$s=f(\psi) \tag{11b}$$

in terms of which the mesh is uniform. The functions $f(\psi)$ and $g(\phi)$ are specially chosen to give the desired distribution of mesh points in the potential plane, while retaining the simplicity and numerical stability of a uniform mesh in the $(t,s)$ computational plane. The derivatives in the potential plane are easily related to those in the computational plane, e.g.

$$P_\phi = g' P_t \tag{12a}$$

$$P_{\phi\phi} = g'' P_t + g'^2 P_{tt} \tag{12b}$$

with analogous formulas for the $\psi$-derivatives. The form of the potential equation thus becomes identical to Eq. (10), with $\phi$ replaced by $t$ and $\psi$ by $s$.

The value of $P$ at any mesh point is represented in the notation $P_{i,j}=P(i\Delta t, j\Delta s)$ where $\Delta t$, $\Delta s$ are the (uniform) mesh spacings in the $t$ and $s$ directions, respectively. Derivatives in the $s$-direction are represented by centered, second-order differences at all internal (i.e., nonboundary) mesh points:

$$(P_s)_{i,j} = \frac{P_{i,j+1}-P_{i,j-1}}{2\Delta s} \tag{13a}$$

$$(P_{ss})_{i,j} = \frac{P_{i,j+1}-2P_{i,j}+P_{i,j-1}}{(\Delta s)^2} \tag{13b}$$

Analogous formulas are used for $t$-derivatives at points in the field for which the local type is elliptic (i.e., where $PF>0$). Such formulas would incorrectly represent the limited domains of influence and dependence in regions of locally hyperbolic type, however. For mesh points in these regions (i.e., where $PF<0$), the second-order operator is skewed to the upstream side of the point:

$$(P_{tt})_{i,j} = \frac{P_{i,j}-2P_{i-1,j}+P_{i-2,j}}{(\Delta t)^2} \tag{14}$$

This operator is only first-order accurate and introduces a dissipative truncation error into the solution in supersonic regions which is sufficient to render the solution stable and unique.

Boundary conditions on both the main airfoil and the slat are treated by incorporating second-order accurate, finite-difference representations of Eqs. (7) and (9) into the differencing formulas at points lying on those boundaries. On the surface of the main airfoil, Eqs. (7) and (13) combine to give, on the upper body surface streamline $j=j_u$

$$(P_s)_{i,j_u} = \frac{P_{i,j_u+1}-P_{i,j_u-1}}{2\Delta s} = 0 \tag{15}$$

whence

$$(P_{ss})_{i,j_u} = \frac{2(P_{i,j_u+1}-P_{i,j_u})}{(\Delta s)^2} \tag{16a}$$

which does not involve the value of $P$ at the necessarily fictitious point $(i,j_u-1)$ which lies "inside" the body. Similarly, along the lower body streamline, $j=j_l$, we have

$$(P_{ss})_{i,j_l} = \frac{-2(P_{i,j_l}-P_{i,j_l-1})}{(\Delta s)^2} \tag{16b}$$

At points lying on the slit representing the slat, the boundary condition is not homogeneous, but is treated in a similar manner. Thus, if $j=j_s$ is the streamline along which the slat boundary conditions are to be applied, we have from Eqs. (9)

$$P_s^+ = \frac{1}{M_\infty^2 f'} \tan\theta^+ \tag{17a}$$

$$P_s^- = \frac{1}{M_\infty^2 f'} \tan\theta^- \tag{17b}$$

and

$$(P_{ss})^+_{i,j_s} = \frac{2(P_{i,j_s+1}-P_{i,j_s}-(\Delta s/M_\infty^2 f')\tan\theta^+)}{(\Delta s)^2} \tag{18a}$$

$$(P_{ss})^-_{i,j_s} = \frac{-2[P_{i,j_s}-P_{i,j_s-1}-(\Delta s/M_\infty^2 f')\tan\theta^-]}{(\Delta s)^2} \tag{18b}$$

This treatment of the body surface boundary points is second-order accurate, and guarantees that the partial differential equation itself (Eq. 4) is satisfied on the slat and airfoil boundaries. This is especially important as the region near the bodies is one of very large gradients.

The farfield boundary condition, Eq. (8), is applied at points on a rectangular boundary in the computational plane, located a finite distance from the airfoil image. Thus, once the value of the circulation constant $\Gamma_t$ has been determined at any stage in the solution process, the values of $P$ at these artificial boundary points are given by

$$P_{i,j} = -\frac{\Gamma_t}{2\pi} \arctan\left[\frac{\beta\psi_j}{\phi_i}\right] \tag{19}$$

The discontinuity in $P$ in crossing the real axis downstream of the trailing edge of the main airfoil is handled by adding (or subtracting) the constant $\Gamma_t$ to the values of $P$ required in the difference equation when the equation spans the slit. The discontinuity is constant only in the physical plane; an interpolation is necessary to find the value of $P$ at the neighboring point above or below the slit. The discontinuity in $P$ across the slit joining the airfoil and slat is similarly handled by adding (or subtracting) the constant $\Gamma_s$ to those values of $P$ required when the difference equation spans the slit. In this case no interpolation is required since the mapping to the physical plane is continuous.

#### Relaxation Solution

The procedure of the previous section results in a system of algebraic equations for the values of $P_{i,j}$ at each of the mesh points in the computational plane. The difficulty in solving these equations arises from two sources: 1) the number of mesh points is generally large, so that even if the system were linear, direct inversion of the coefficient matrix would be inefficient, and 2) the system is not linear, the nonlinearity arising not only from the form of the finite difference equation, but from the fact that $\Gamma_f$ and $\Gamma_s$ are a priori unknown. Both of these difficulties suggest that an iterative solution is appropriate.

The equations first are linearized by considering as unknown only those quantities appearing in the highest order differences, using values from the previous iteration for the remaining quantities. The resulting linear system is solved by successive line overrelaxation along lines of constant $t$, sweeping the field in the downstream direction. From the computed values of surface pressure near the trailing edges of the slat and the main airfoil, the constants $\Gamma_s$ and $\Gamma_f$ are adjusted until the upper and lower surface values agree. This is done continuously, i.e., after each sweep through the field, $\Gamma_s$ and $\Gamma_f$ are changed by an amount which locally forces the Kutta condition to be approximately satisfied. As the solution progresses towards convergence, the changes in these values become smaller and smaller, as does the deviation from the exact satisfaction of the Kutta condition.

## Results

Two major questions regarding the validity of the proposed theory might be posed. The first regards the ability of the small-disturbance formulation to accurately represent supercritical flowfields with or without shock waves; the second regards the ability of the thin-airfoil representation of the slat to realistically model its effects on the flowfield. The first question can be answered by comparing results of the present calculations for single airfoils with those of exact hodograph methods for special (shockfree) cases, and with results of more exact solutions of the complete potential equation for more general cases (e.g., for those cases involving shock waves). For the second question, no such definitive comparison can be made, since no exact potential solutions are available for multi-element airfoils in the transonic regime. In order to compare with potential solutions, we are forced into the incompressible regime where accepted "exact" solutions do exist for multiple bodies; comparisons at transonic speeds are limited to those with experimental data (for which the influence of viscous and/or wind-tunnel-wall effects are not always well-known).

The results of a number of calculations addressing these questions will now be presented. In all cases, the results were computed on a mesh with about 100 axially and 40 laterally distributed points, including approximately 120 points on the surface of the main airfoil. The slat surface was generally represented by fewer than 20 points, but this number seemed sufficient if the location of points near the nose of the slat were chosen carefully. The outer boundaries of the computational region were chosen approximately 3 chordlengths above and below the airfoil. Convergence for a given set of conditions is generally achieved in 200-300 iterations, requiring about 3 min of CPU time on the CDC 6600 computer for which the program requires 70K (octal) of high-speed core. An additional minute or so of CPU time is required to perform the preliminary mappings for each geometrical configuration to be studied.

#### Validity of Small-Disturbance Theory

The results of several calculations for the transonic flow about single-element airfoils will be presented to illustrate the ability of the basic small-disturbance theory to accurately predict the potential flowfield in such cases. First we show a comparison of results for the so-called Korn airfoil, which has a rather large supercritical region designed to achieve isentropic recompression. Such shockfree airfoils provide a particularly sensitive test of accuracy as slight inaccuracies in the solution are generally magnified in the recompression region, resulting in the appearance of shock waves. Figure 4 compares results for the surface pressure distribution on the airfoil of the present method with those of the hodograph design procedure of Korn and Garabedian.[10] The present theory shows a weak shock at the end of the recompression region, but agreement is generally good.

Figure 5 is included to demonstrate the ability of the theory to accurately predict flowfields with rather strong shock waves. The results of the present method are compared with those of the Korn and Garabedian analysis program,[10] which solves the finite-difference form of the complete potential

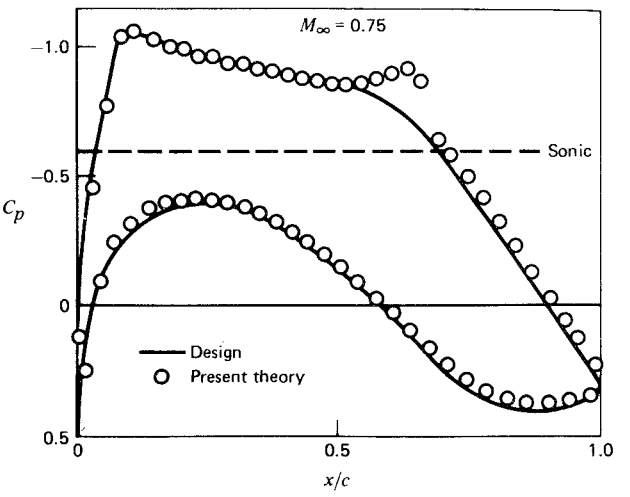


**Fig. 4 Surface pressure distribution on Korn airfoil at design conditions.**

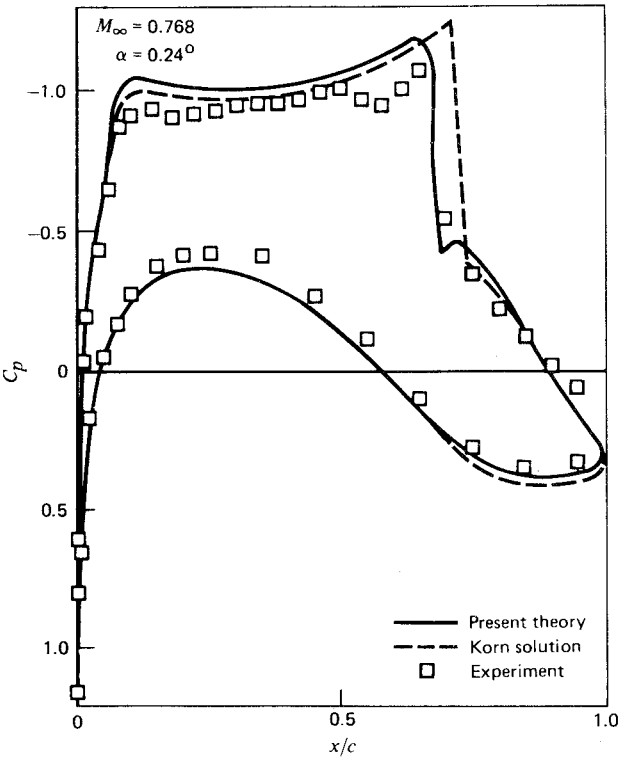


**Fig. 5 Surface pressure distribution on Korn airfoil at off-design point.**

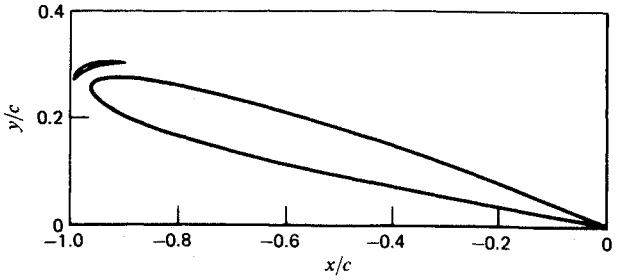


**Fig. 6 Geometry for incompressible test case.**

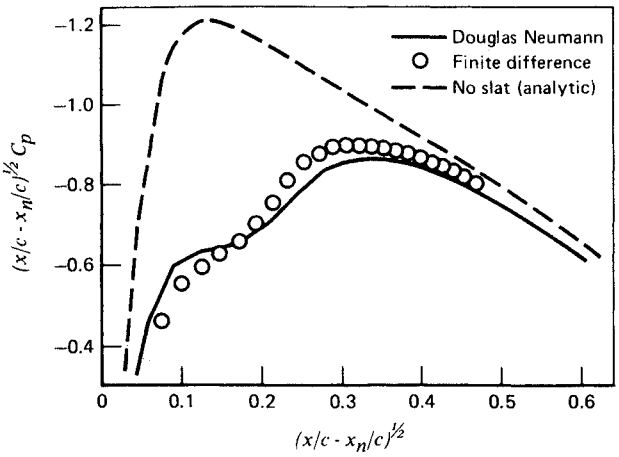


**Fig. 7a Slat surface pressure distribution for incompressible test case.**

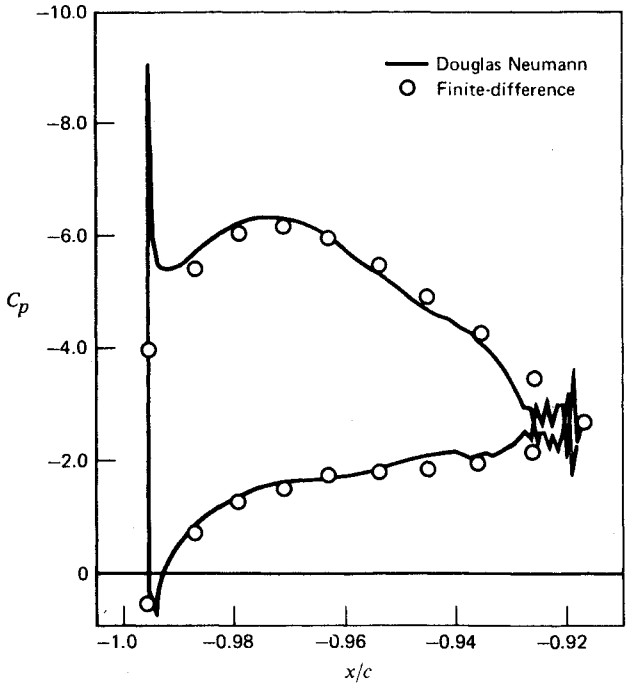


**Fig. 7b Main airfoil surface pressure distribution (modified) for incompressible slat test case.**

equation. The surface pressure distribution is shown for the Korn airfoil at an off-design point; the airfoil is at an angle of attack of 0.24° in a flow with freestream Mach number of 0.768, and produces a nearly normal shock of upstream Mach number slightly greater than 1.3 at the body surface. Also included are the results of a high-Reynolds-number experiment,[10] which indicates the good agreement obtainable with inviscid theories for well-designed airfoils. Again the

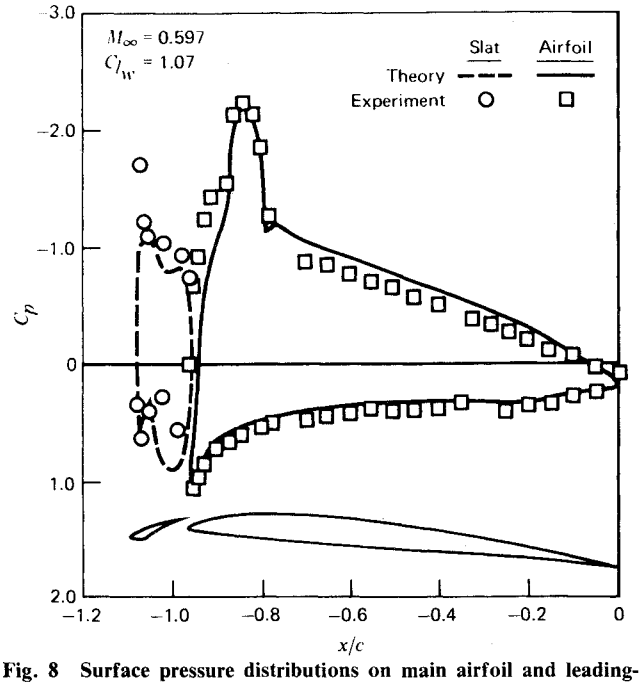


**Fig. 8 Surface pressure distributions on main airfoil and leading-edge slat.**

agreement between the results of the present theory and the solution of the complete potential equation is quite good.

### Validity of Slat Treatment

To test the efficacy of the linearized treatment of the slat boundary conditions, solutions using the present method were compared with "exact" solutions obtained using the Douglas Neumann Program surface singularity method[1] for several incompressible test cases. A sample of these comparisons for the geometry of Fig. 6 is shown in Figs. 7a and 7b. For this case the slat was chosen to be a completely general test of the theory in that it has angle of attack and camber as well as thickness, relative to the coordinate line along which the boundary conditions are applied. Note that the pressure distribution plot of Fig. 7b has been modified to incorporate a square-root scaling, designed to better depict the suction peak on the main airfoil. Also shown is the pressure distribution on the main airfoil in the absence of the slat to indicate the magnitude of its effect. Agreement is seen to be excellent for both the slat and main airfoil pressure distributions, except for details finer than the resolution of the finite difference mesh could hope to capture. The solutions are relatively insensitive to the precise location of the line chosen to represent the slat, which is consistent with the concept of the mean-surface approximation used in applying the slat boundary conditions. The stretching of the mesh in the lateral direction can always be adjusted to place one of the coordinate lines near the slat, however; in practice, the coordinate line has usually been chosen to pass through the slat trailing edge.

### Comparisons with Experimental Data

Finally, some comparisons with experimental data for slatted configurations taken in the transonic speed regime will be presented. The experimental data[11] were obtained at a Reynolds number of about $2 \times 10^7$ in the two-dimensional insert of the NAE 5-ft Blowdown Tunnel at Ottawa, Ontario. The model tested was an NACA 64A-406 airfoil, modified to have a retractable leading-edge slat of 13.5% chord. The part line between the slat and main airfoil was designed to give the main airfoil the same leading-edge radius when the slat was extended as that of the original profile. Tests were run at various angles of attack for several positions of the slat relative to the main airfoil. The leading-edge configuration of one such geometry is shown in Fig. 1.

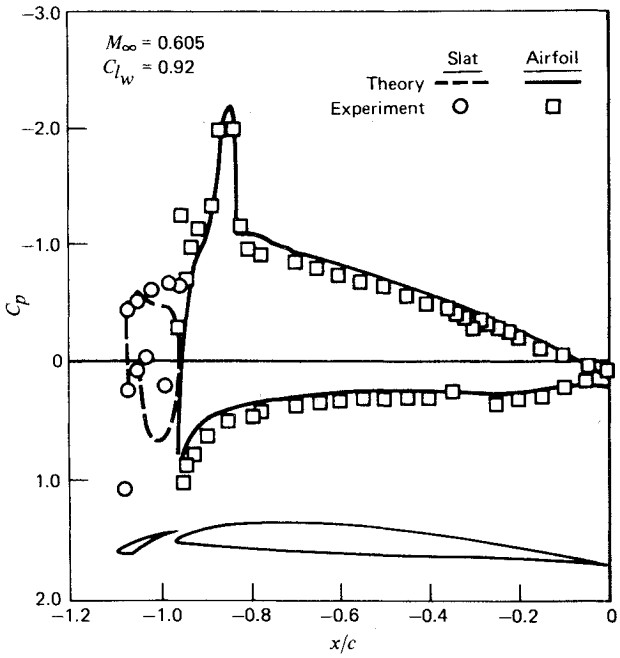


**Fig. 9 Surface pressure distributions on main airfoil and leading-edge slat.**

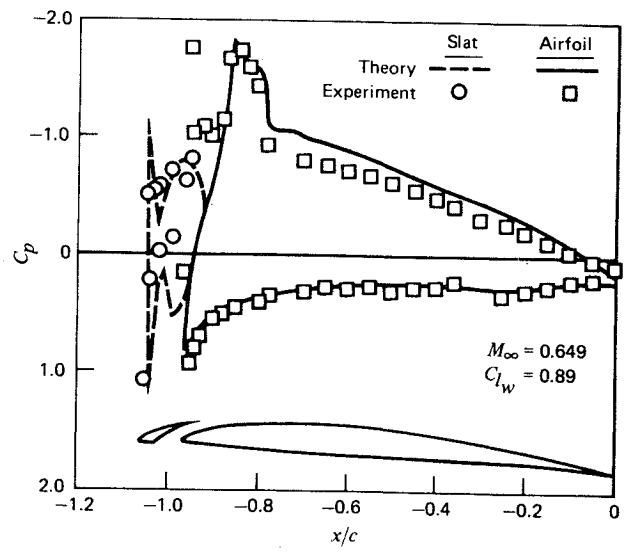


**Fig. 10 Surface pressure distributions on main airfoil and leading-edge slat.**

For these comparisons, first-order viscous effects on the main airfoil were accounted for by adding the displacement thickness corresponding to a canonical pressure distribution to the physical ordinates of the airfoil. Also, since the effective angle of attack of the model in the tests was uncertain, results are compared for the same value of lift coefficient on the main airfoil. In general, agreement between the calculated results and the experiment was quite good for those cases in which viscous effects on the slat were not judged to be too important. The results of two such cases are shown in Figs. 8 and 9. A third case, for which viscous effects on the slat are probably important is shown in Fig. 10. Here the after portion of the lower slat surface is thought to be badly separated, as is evidenced by the lack of pressure recovery there which would be expected due to its high camber. The incorrect modeling of the effect of the slat separation also results in poor agreement near the leading edge of the main airfoil.

## Conclusions

The method presented here seems to offer promise for analyzing the flow about airfoils with leading-edge slats in the transonic regime for cases in which viscous forces do not play a major role. It has been shown in studies of the incompressible flow about multi-element airfoils, that relatively straightforward corrections for viscous effects, such as the addition of boundary-layer displacement thicknesses, to define a new effective geometry, results in much-improved agreement with experimental data.[12-14] Similar improvements might be expected if the present theory were corrected systematically for these effects, and this is one area which warrants further study. On the other hand, it might be supposed that since the primary purpose of the maneuvering slat is to allow high lift to be achieved at low values of drag, efficient designs will be those which do not allow substantial separated zones to exist. Thus, the method is already capable of treating many cases of practical interest.

## References

[1] Hess, J. L. and Smith, A.M.O., "Calculation of Potential Flow about Arbitrary Bodies," *Progress in Aeronautical Sciences,* Vol. 8, Pergamon Press, New York, 1966, pp. 1-138.

[2] O'Pray, J.E. and Lissaman, P.B.S., "Leading-Edge Slat Design by a Semi-Inverse Technique," *Journal of Aircraft,* Vol. 9, Feb. 1972, pp. 143-149.

[3] Liebeck, R.H., "Theoretical Studies on the Aerodynamics of Slat-Airfoil Combinations," Rept. MDC J5195, May 1971, Douglas Aircraft Co., Long Beach, Ca.

[4] McGregor, O.W. and McWhirter, J.W., "Development of Theoretical Method for Two-dimensional Multi-element Airfoil Analysis and Design, Part II: Leading-Edge Slat Design Method," TR-72-96, Part II, 1972, Air Force Flight Dynamics Lab., Wright-Patterson AFB, Ohio.

[5] James, R.M., "Analytical Studies of Two-element Airfoil Systems," Rept. MDC J5831, Feb. 1974, Douglas Aircraft Co., Long Beach, Ca.

[6] Caughey, D.A., "A New Transonic Small-Disturbance Theory for Numerical Analysis," Rept. MDC Q0478, Dec. 1972, McDonnell Douglas, St. Louis, Mo.

[7] Hayes W.D., "La seconde approximation pour les ecoulements transsoniques nonvisqueux," *Journal de Mechanique,* Vol. 5, 1966, pp. 163-206.

[8] James, R.M., "A New Look at Two-dimensional Incompressible Airfoil Theory," Rept. MDC J0918, May 1971, Douglas Aircraft Co., Long Beach, Ca.

[9] Murman, E.M. and Cole, J.D., "Calculation of Plane, Steady, Transonic Flows," *AIAA Journal,* Jan. 1971, pp. 114-121.

[10] Kacpryzynski, J.J., Ohman, L.H., Garabedian, P.R., and Korn, D.G., "Analysis of the Flow Past a Shockless Lifting Airfoil in Design and Off-design Conditions," AIAA Paper 71-567, 1971.

[11] Durando, N.A. and Tranen, T.L., "Investigation of Conventional and Advanced Airfoil Sections, Including High-Lift Devices for Transonic Maneuverability," EN906, 1972, McDonnell Aircraft Co., St. Louis, Mo.

[12] Stevens, W.A., Goradia, S.H., and Braden, J.A., "Mathematical Model for Two-dimensional Multi-component Airfoils in Viscous Flow," NASA CR-1843, 1971.

[13] Bhateley, I.C. and McWhirter, J.W., "Development of Theoretical Method for Two-dimensional Multielement Airfoil Analysis and Design, Part I: Viscous Flow Analysis Method," TR-72-96, Part I, 1972, Air Force Flight Dynamics Lab., Wright-Patterson AFB, Ohio.

[14] Callaghan, J.G. and Beatty, T.D., "A Theoretical Method for the Analysis and Design of Multielement Airfoils," *Journal of Aircraft,* Vol. 9, Dec. 1972, pp. 844-848.